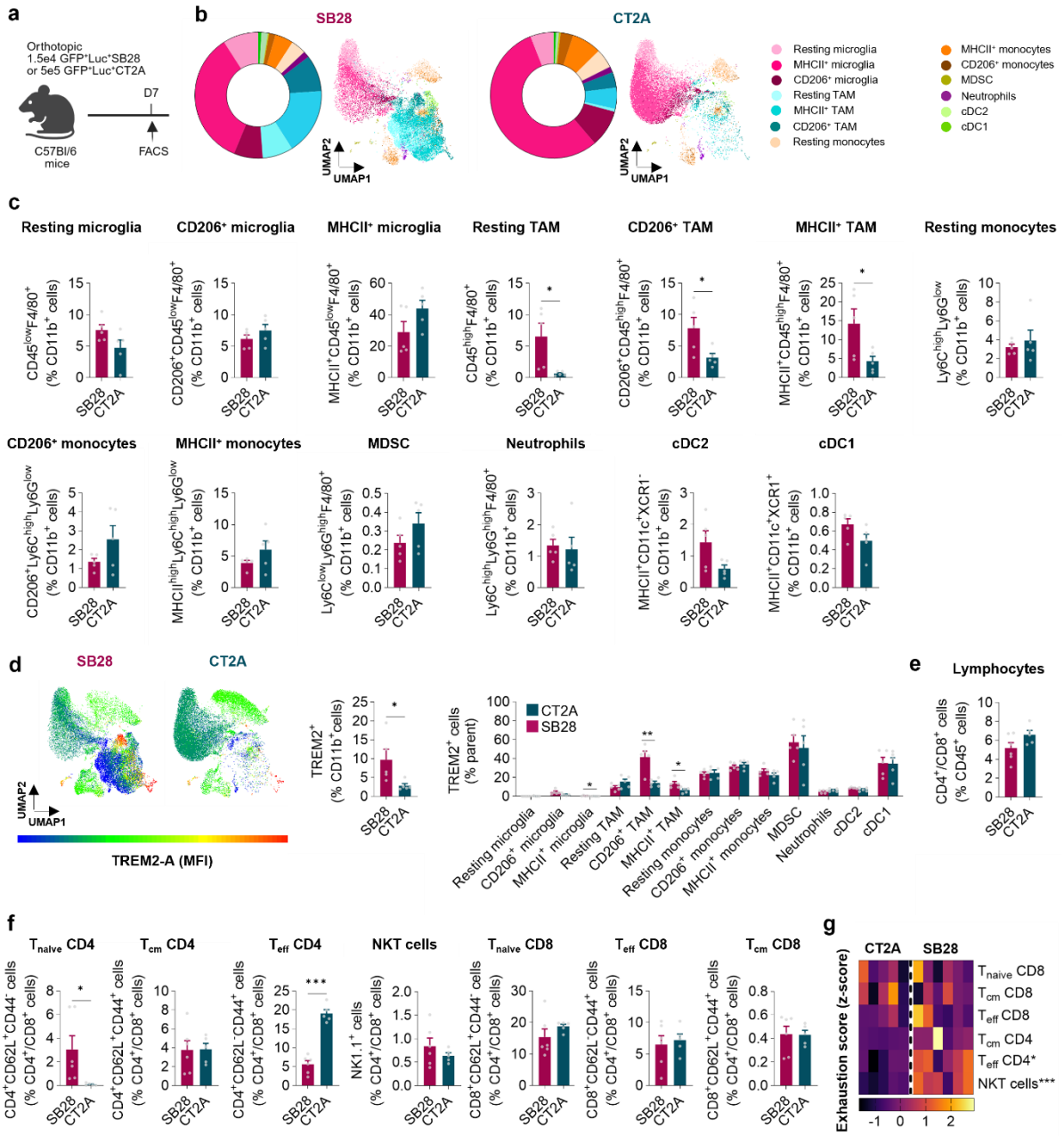

Supplemental figure 1. Baseline immune landscape of SB28 and CT2A tumors prior to resection. (**a**) Experimental scheme comparing orthotopic CT2A and SB28 tumors on TME at day 7 (D7) by flow cytometry. (**b**) Uniform manifold approximation and projection (UMAP) visualization of flow cytometry analysis of $CD45^+CD11b^+$ myeloid populations and donut charts showing the distribution of major myeloid subsets in CT2A and SB28 tumors at D7. (**c**) Frequency of microglial, dendritic cell (cDC1 and cDC2), myeloid-derived suppressor cells (MDSC), neutrophil, tumor-associated macrophage (TAM), and monocyte subsets in CT2A vs SB28 tumors, shown as percentage of $CD11b^+$ cells (n=5 mice per group). (**d**) UMAP visualization of flow cytometry analysis of $CD45^+CD11b^+$ myeloid population colored by TREM2 expression intensity in SB28 and CT2A tumors (left panel). Frequency of $TREM2^+$ cells among total $CD11b^+$ myeloid cells in SB28 and CT2A tumors, and distribution of TREM2 expression across individual myeloid subsets (right panel) (n=5 mice per group). (**e**) Frequency of total $CD4^+/CD8^+$ lymphocytes among $CD45^+$ cells in SB28 and CT2A tumors. (**f**) Frequency of lymphoid subsets, including $CD4^+$ and $CD8^+$ naïve (T_{naive}), central memory (T_{cm}), and

effector (T_{eff}) populations, as well NKT cells, expressed as percentages of $CD4^+/CD8^+$ in SB28 and CT2A tumors at D7 (n=5-6 mice per group). (**g**) Heatmap showing exhaustion scores (z-scores; see Methods) for indicated lymphoid subsets in SB28 and CT2A tumors at D7. Data are shown as mean ± SEM with individual data points representing mice (n = 5-6 per group). Statistical analyses were performed using unpaired two-tailed t-tests. *$p < 0.05$, **$p < 0.01$, ***$p < 0.001$.

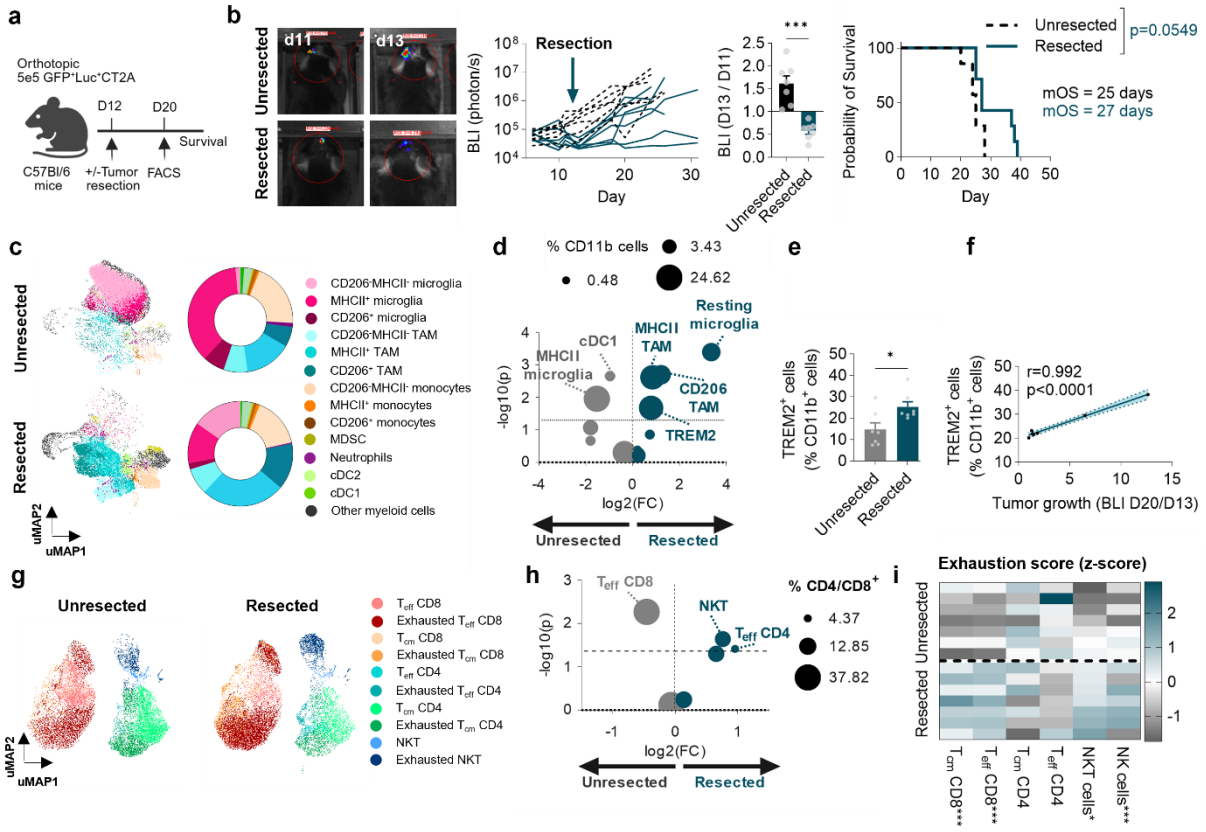

Supplemental figure 2. Tumor resection induces delayed myeloid remodeling and TREM2 upregulation in orthotopic CT2A model. (**a**) Experimental scheme comparing unresected and resected orthotopic CT2A tumors on TME at day 20 (D20) by flow cytometry. (**b**) Left to right: representative bioluminescence imaging (BLI) at days 11 and 13 post-implantation, longitudinal BLI quantification, comparison of BLI signal between days 10 and 11, and Kaplan–Meier survival analysis of unresected and resected mice (log-rank test). mOS=median of survival. (**c**) Uniform manifold approximation and projection (UMAP) visualization of flow cytometry analysis of $CD45^+CD11b^+$ myeloid populations and donut charts showing the distribution of major myeloid subsets in unresected and resected CT2A tumors. (**d**) Volcano plot showing differential abundance of myeloid populations between unresected and resected CT2A tumors; dot size reflects mean population frequency. (**e**) Frequency of $TREM2^+$ cells among $CD11b^+$ myeloid cells in unresected and resected CT2A tumors (mean ± SEM, n = 6–7 mice per group). (**f**) Pearson correlation between $TREM2^+$ myeloid cell frequency and tumor growth (BLI ratio D20/D11) in the CT2A model; shaded area indicates 95% confidence interval. (**k**) UMAP visualization of $CD45^+$ lymphoid populations in unresected and resected SB28 tumors. (**l**) Volcano plot of differential lymphoid population abundance between unresected and resected SB28 tumors. (**m**) Heatmaps showing exhaustion scores (z-scores; see Methods) for indicated lymphoid subsets in unresected and resected tumors in CT2A model (n = 7 mice per group). Data are shown as mean ± SEM unless indicated. Unpaired or paired two-tailed t-tests were used as appropriate. *p < 0.05, ***p < 0.001.

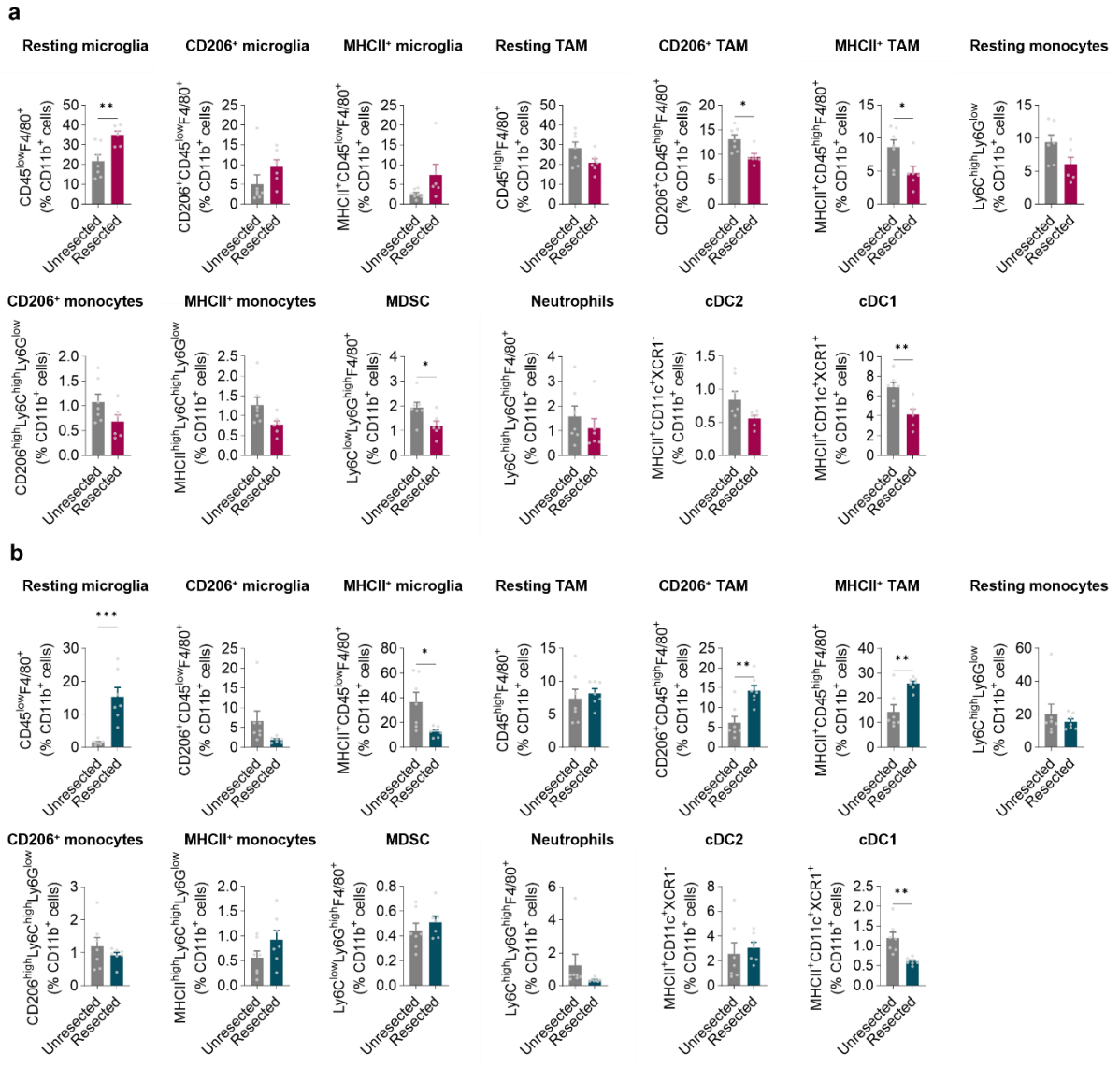

Supplemental figure 3. Tumor resection induces delayed myeloid remodeling in orthotopic GBM models. (**a**) Frequency of microglial, dendritic cell (cDC1 and cDC2), myeloid-derived suppressor cells (MDSC), neutrophil, tumor-associated macrophage (TAM), and monocyte subsets in unresected vs resected SB28 tumors, shown as percentage of $CD11b^+$ cells. (**b**) Frequency of microglial, dendritic cell (cDC1 and cDC2), myeloid-derived suppressor cells (MDSC), neutrophil, tumor-associated macrophage (TAM), and monocyte subsets in unresected vs resected CT2A tumors, shown as percentage of $CD11b^+$ cells. Data are shown as mean ± SEM with individual data points representing mice (n=6–7 per group). Statistical analyses were performed using unpaired two-tailed t-tests. *$p < 0.05$, **$p < 0.01$, ***$p < 0.001$.

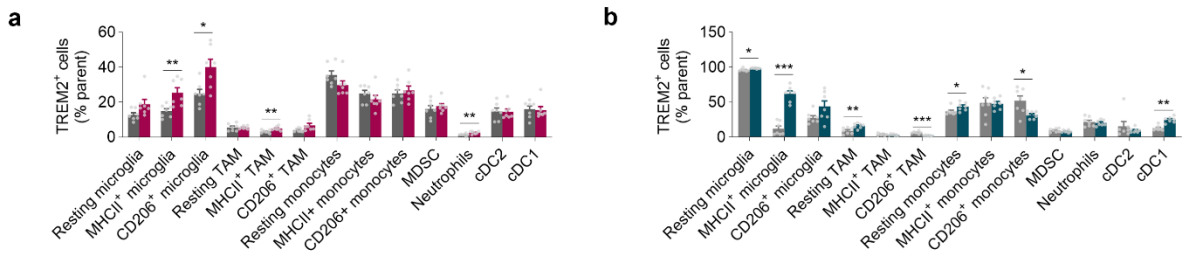

Supplemental figure 4. Tumor resection induces TREM2 upregulation in orthotopic GBM models. (**a**) Distribution of TREM2$^+$ cells across individual myeloid cell subsets in SB28 tumors at day 20. (**b**) Distribution of TREM2$^+$ cells across individual myeloid cell subsets in CT2A tumors at day 20. Data are shown as mean ± SEM with individual data points representing mice (n=6–7 per group). Statistical analyses were performed using unpaired two-tailed t-tests. *p < 0.05, **p < 0.01, ***p < 0.001.

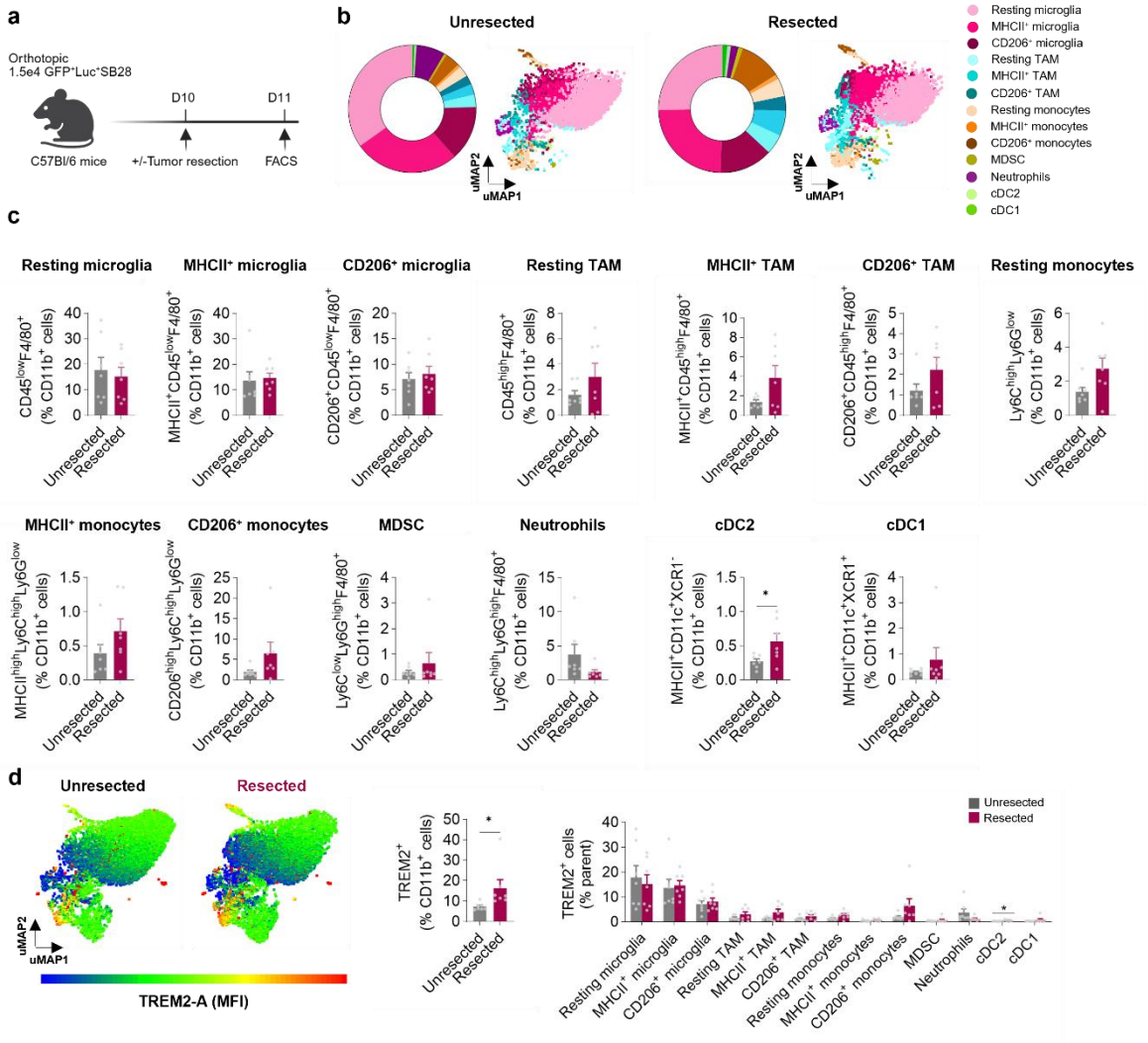

Supplemental figure 5. Tumor resection induces acute myeloid remodeling and TREM2 upregulation in orthotopic SB28 model. (**a**) Experimental scheme comparing unresected and resected orthotopic SB28 tumors on TME at day 11 (D11) by flow cytometry. (**b**) Uniform manifold approximation and projection (UMAP) visualization of flow cytometry analysis of $CD45^+CD11b^+$ myeloid populations and donut charts showing the distribution of major myeloid subsets in unresected and resected SB28 tumors. (**c**) Frequency of microglial, dendritic cell (cDC1 and cDC2), myeloid-derived suppressor cells (MDSC), neutrophil, tumor-associated macrophage (TAM), and monocyte subsets in unresected vs resected SB28 tumors at D11, shown as percentage of $CD11b^+$ cells. (**d**) UMAP visualization of flow cytometry analysis of $CD45^+CD11b^+$ myeloid population colored by TREM2 expression intensity in unresected vs resected SB28 tumors at D11 (left panel). Frequency of $TREM2^+$ cells among total $CD11b^+$ myeloid cells in unresected vs resected SB28 tumors at D11, and distribution of TREM2 expression across individual myeloid subsets (right panel). Data are shown as mean ± SEM with individual data points representing mice (n=7 per group). Statistical analyses were performed using unpaired two-tailed t-tests. *$p < 0.05$, **$p < 0.01$, ***$p < 0.001$.

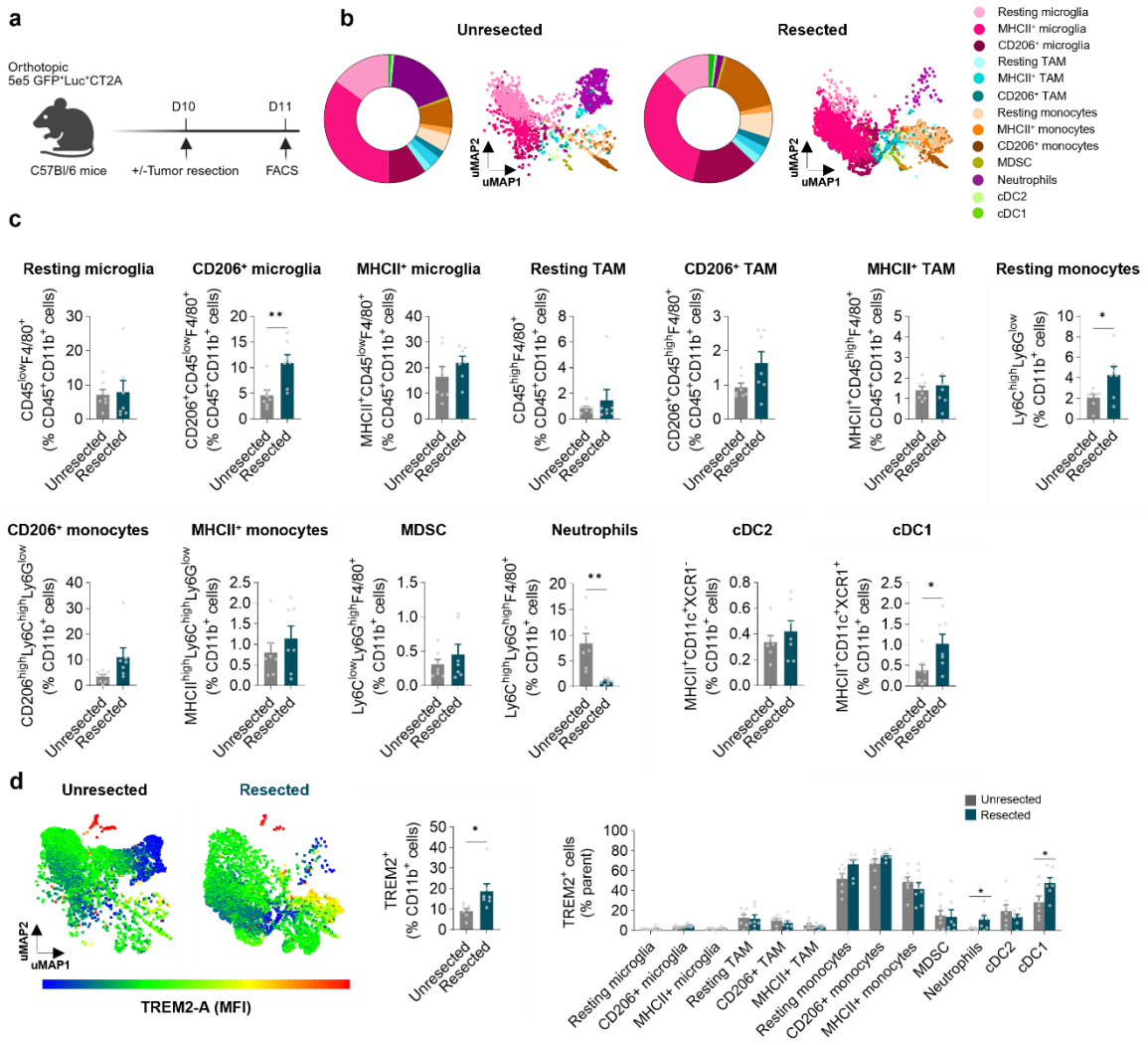

Supplemental figure 6. Tumor resection induces acute myeloid remodeling and TREM2 upregulation in orthotopic CT2A model. (**a**) Experimental scheme comparing unresected and resected orthotopic CT2A tumors on TME at day 11 (D11) by flow cytometry. (**b**) Uniform manifold approximation and projection (UMAP) visualization of flow cytometry analysis of $CD45^+CD11b^+$ myeloid populations and donut charts showing the distribution of major myeloid subsets in unresected and resected CT2A tumors. (**c**) Frequency of microglial, dendritic cell (cDC1 and cDC2), myeloid-derived suppressor cells (MDSC), neutrophil, tumor-associated macrophage (TAM), and monocyte subsets in unresected vs resected CT2A tumors at D11, shown as percentage of $CD11b^+$ cells. (**d**) UMAP visualization of flow cytometry analysis of $CD45^+CD11b^+$ myeloid population colored by TREM2 expression intensity in unresected vs resected CT2A tumors at D11 (left panel). Frequency of $TREM2^+$ cells among total $CD11b^+$ myeloid cells in unresected vs resected CT2A tumors at D11, and distribution of TREM2 expression across individual myeloid subsets (right panel). Data are shown as mean ± SEM with individual data points representing mice (n=7 per group). Statistical analyses were performed using unpaired two-tailed t-tests. *$p < 0.05$, **$p < 0.01$, ***$p < 0.001$.

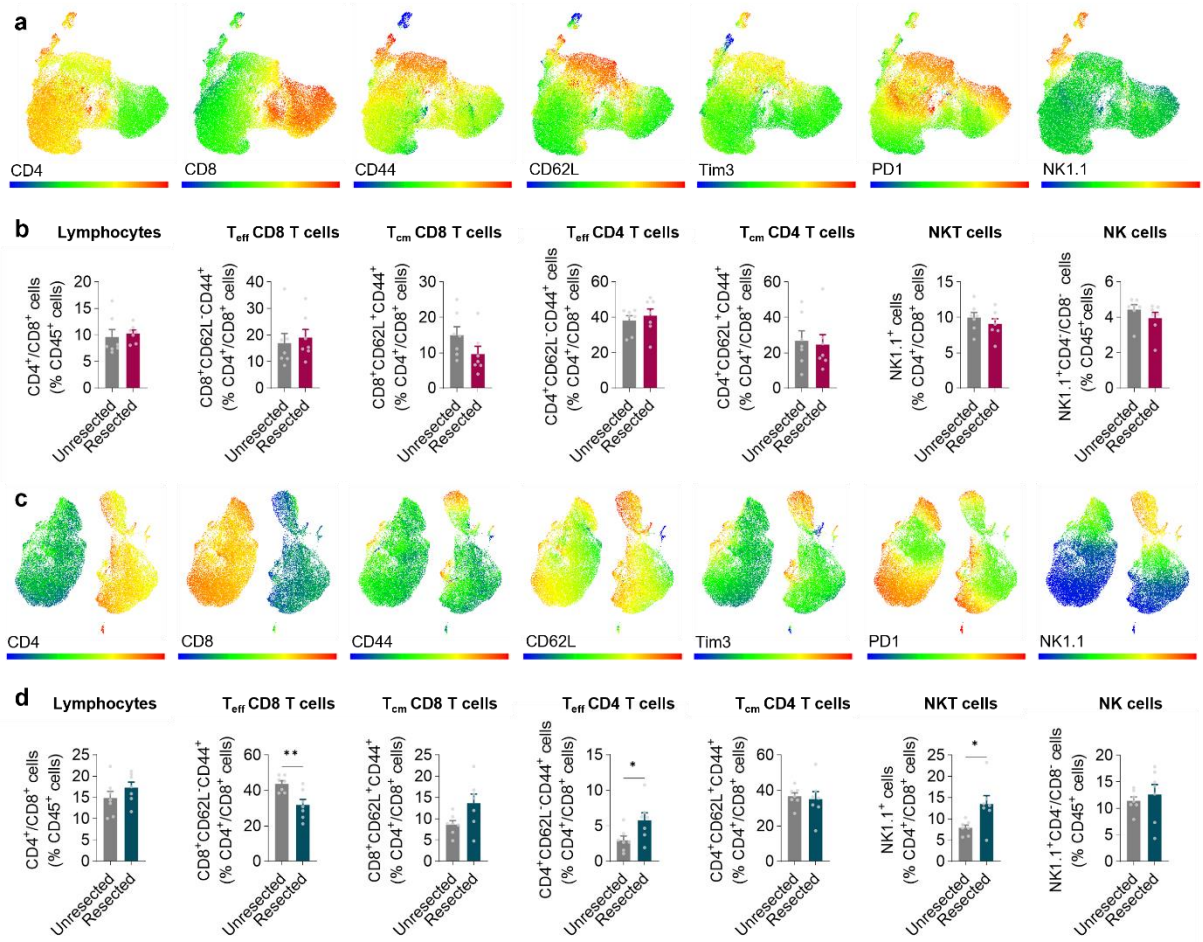

Supplemental figure 7. Expression intensity of T-cell markers in resected and unresected glioblastomas in lymphoid cell populations ten days after resection in SB28 and CT2A tumors. (**a/c**) Uniform manifold approximation and projection (UMAP) visualization of lymphoid cell populations gated as $CD45^+CD3^+$ cells from SB28 (**a**) and CT2A (**c**) tumors. Each dot represents an individual cell colored according to expression intensity of indicated markers (CD4, CD8, CD44, CD62L, Tim3, PD1 and NK1.1). **(c)** Quantification of total lymphocytes, effector (T_{eff}) and central memory (T_{cm}) CD4, T_{eff} and T_{cm} CD8, NKT cells and NK cells in unresected vs resected SB28 (**b**) and CT2A (**d**) tumors. Data are shown as mean ± SEM with individual data points representing mice (n=6-7 per group). Statistical analyses were performed using unpaired two-tailed t-tests. *$p < 0.05$, **$p < 0.01$.

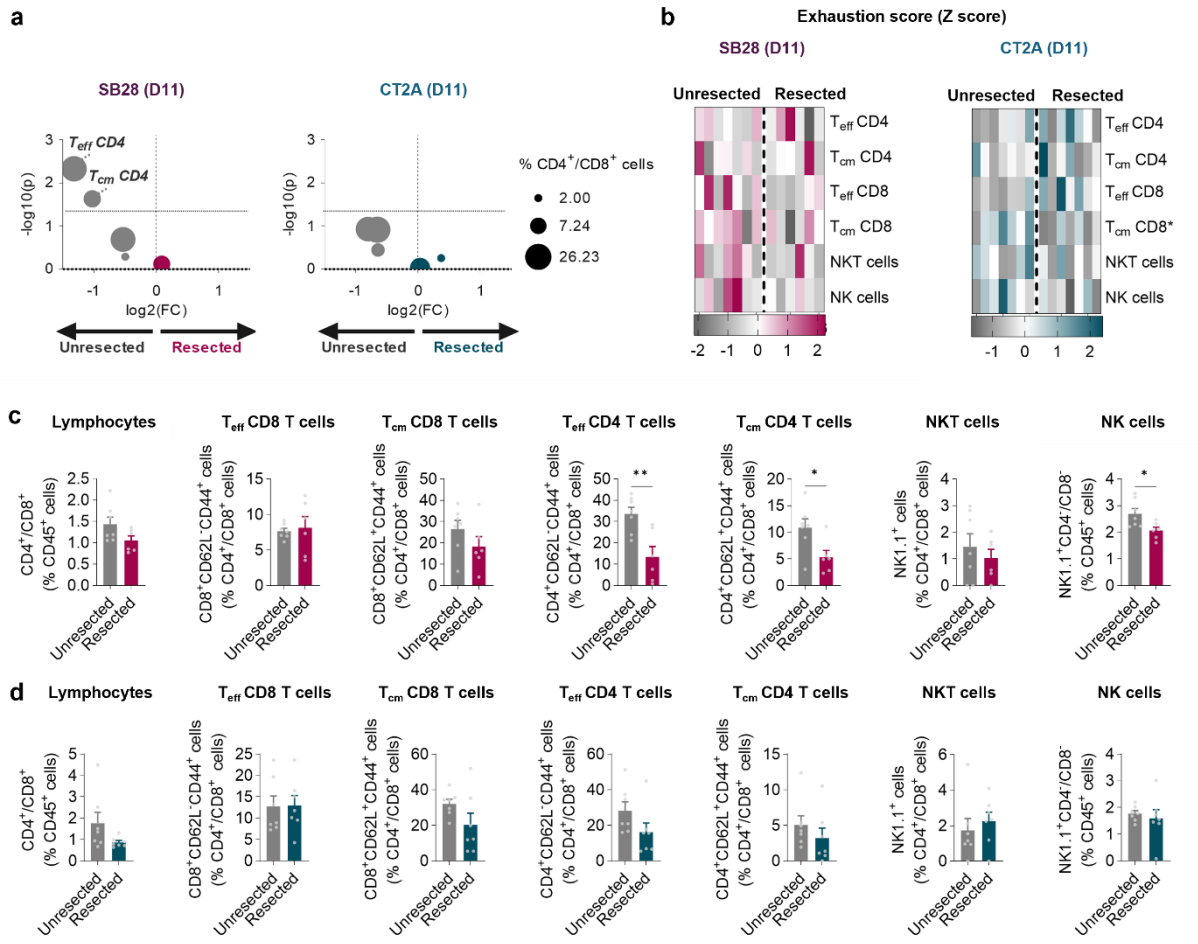

Supplemental Figure 8. Quantification of lymphoid cell populations and exhaustion profiles 10 days after tumor resection in SB28 and CT2A models. (**a**) Volcano plot depicting differences in immune cell population abundance between unresected and resected tumors in SB28 (magenta) or CT2A (dark blue) models, as determined by high-dimensional flow cytometry. The x-axis shows the $\log_2$ fold-change (log2FC) in cell frequency, with positive values indicating enrichment in resected tumors (magenta or dark blue) and negative values indicating enrichment in unresected tumors (grey). The y-axis shows the –log10(p). Circle size is proportional to the mean frequency of each population across samples. (**b**) Heatmaps showing exhaustion scores (see Methods) expressed as z-scores for the indicated lymphoid cell subsets in unresected and resected tumors at day 20 post-implantation in SB28 (left panel) and CT2A (right panel) models. T_{cm}, central memory T cells; T_{eff}, effector T cells; NK, natural killer cells; NKT, natural killer T cells (n=6-7 independent animals per group). Statistical significance was determined using unpaired two-tailed t-tests. *$p < 0.05$, **$p < 0.01$.

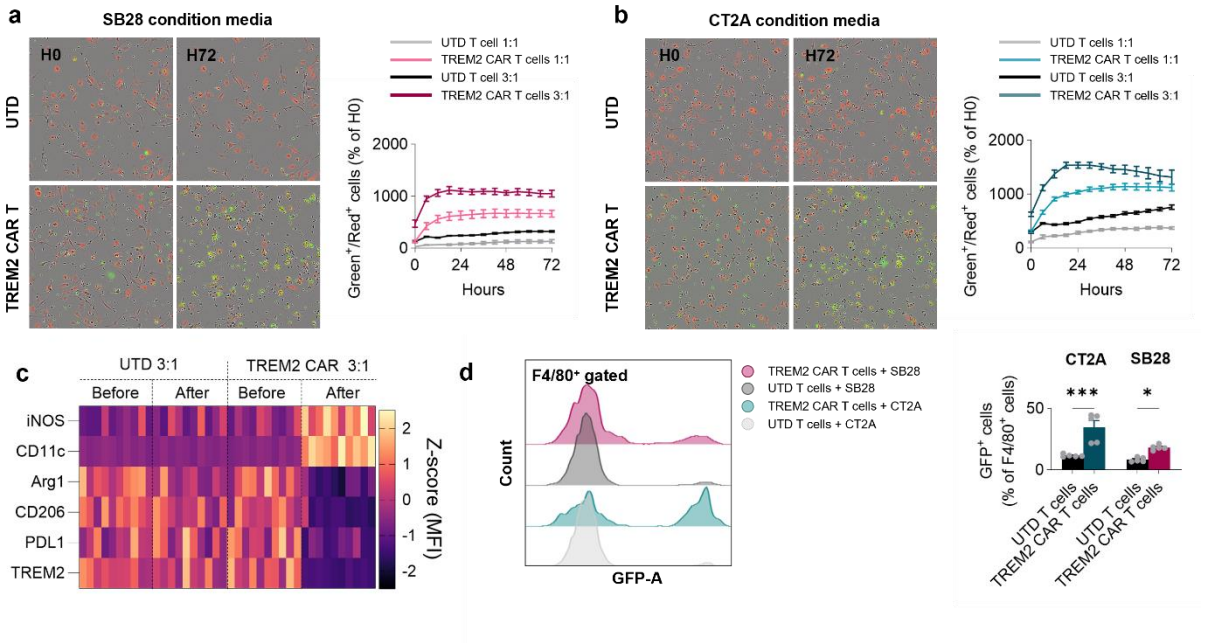

Supplemental Figure 9. Anti TREM2 CAR T cells eliminate and reprogram GBM-conditioned macrophages *in vitro*. (**a-b**) Representative IncuCyte images of bone marrow–derived macrophages (BMDMs) pre-exposed to SB28- (**a**) or CT2A- (**b**) conditioned media (CM) and co-cultured with untransduced (UTD) T cells or anti-TREM2 CAR T cells at an effector-to-target (E:T) ratio of 1:1 or 3:1. Images are shown at the start of co-culture (H0) and after 72 h (H72). BMDMs are labeled with CellTrace Yellow, and dead cells are detected using Cytotox Green. Quantification of macrophage killing over time, expressed as the normalized area of double-positive (CellTrace Yellow$^+$/Cytotox Green$^+$) signal relative to H0, for SB28-CM (**a**) and CT2A-CM (**b**)–conditioned BMDMs co-cultured with UTD or anti-TREM2 CAR T cells (n=3-6 technical replicates per condition). (**c**) Heatmap showing z-scored mean fluorescence intensity (MFI) of indicated markers in F4/80$^+$ BMDMs before and after co-culture with UTD or anti-TREM2 CAR T cells (E:T 3:1). (**d**) Flow cytometry analysis of F4/80$^+$ BMDM showing GFP$^+$ target uptake following a 24 h co-culture with GFP$^+$GD2$^+$ SB28 or CT2A tumor cells after prior exposure to UTD or TREM2 CAR T cells (3:1 E:T ratio). Quantification of the percentage of GFP$^+$ cells within the F4/80$^+$ population is shown on the right (n=independent replicates; one-way ANOVA). Data are shown as mean +/- SEM. *p < 0.05, **p<0.01, ***p<0.001.

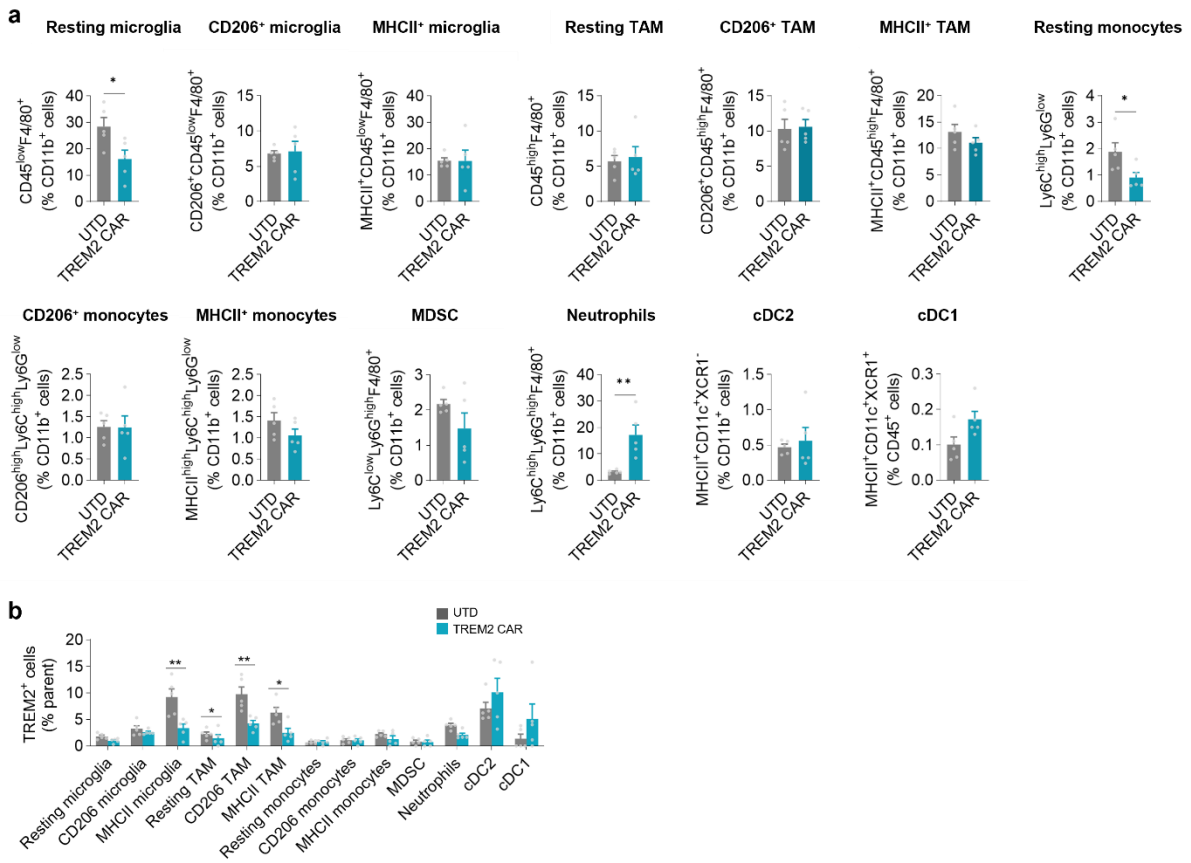

Supplemental figure 10. TREM2 CAR T cells deplete TREM2⁺ myeloid cells and recruit pro-inflammatory neutrophils *in vivo*. (**a**) Frequency of microglial, dendritic cell (cDC1 and cDC2), myeloid-derived suppressor cells (MDSC), neutrophil, tumor-associated macrophage (TAM), and monocyte subsets in resected SB28 tumors treated with UTD or anti-TREM2 CAR T cells (n = 7 mice per group) shown as percentage of $CD45^{+}CD11b^{+}$ cells. (**b**) Distribution of TREM2 expression across individual myeloid subsets in resected SB28 tumors treated with UTD or anti-TREM2 CAR T cells (n=7 mice per group). Data are shown as mean ± SEM. Unpaired two-tailed t-tests were used. *$p < 0.05$, **$p < 0.01$.

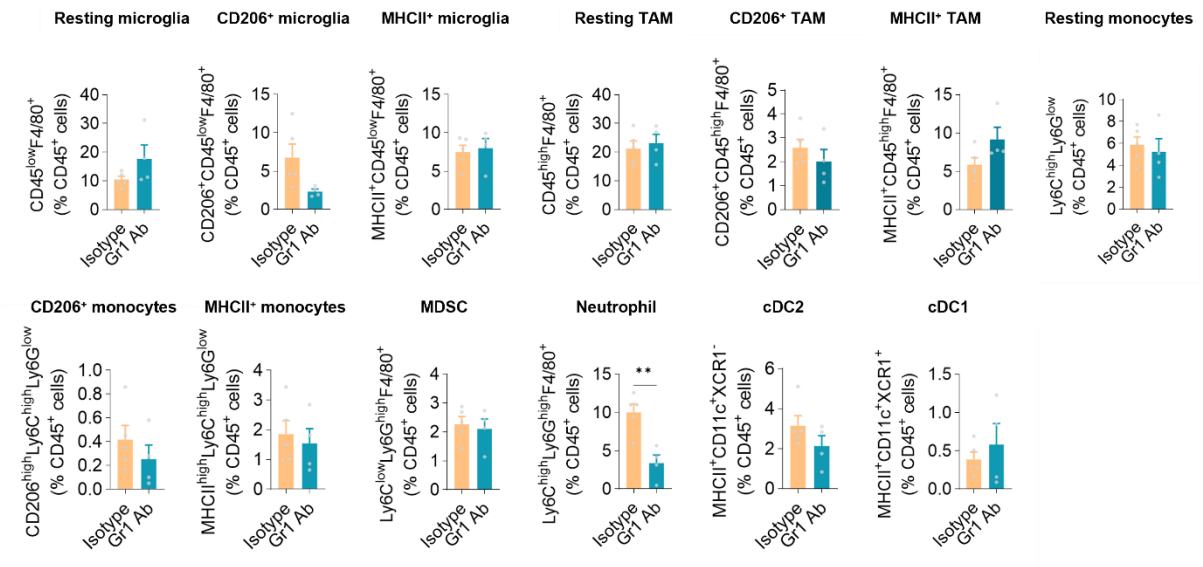

Supplemental figure 11. Impact of neutrophil depletion on myeloid cell compartment composition following TREM2 CAR T-cell therapy. Frequency of microglial, dendritic cell (cDC1 and cDC2), myeloid-derived suppressor cells (MDSC), neutrophil, tumor-associated macrophage (TAM), and monocyte subsets in isotype *versus* anti-Gr1 antibody (Ab)-treated SB28-bearing mice treated with TREM2 CAR T cells shown as percentage of $CD45^+$ cells (n=4-5 mice per group). Data are shown as mean ± SEM. Unpaired two-tailed t-tests were used. *$p < 0.05$, **$p < 0.01$.

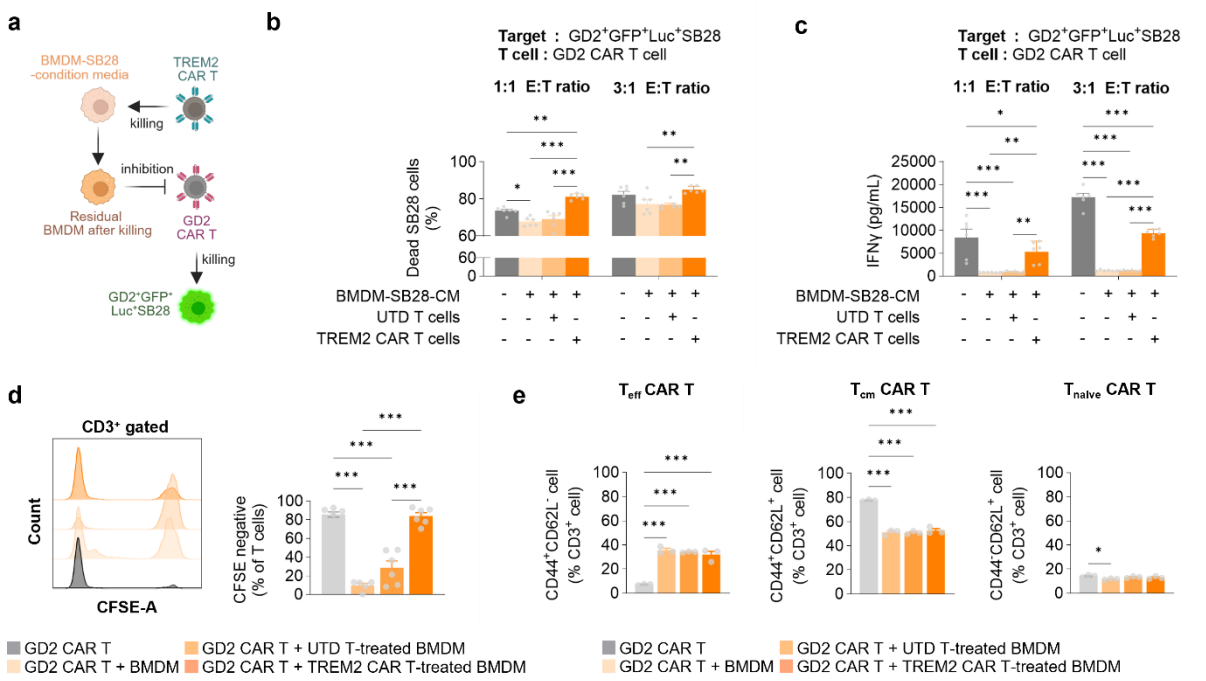

Supplemental figure 12. Impact of TREM2 CAR T cell–conditioned macrophages on GD2-CAR T cell activity. (**a**) Experimental scheme: bone marrow–derived macrophages (BMDM) were pretreated with conditioned medium from SB28 cells (SB28 CM), then exposed to either untransduced (UTD) or TREM2 CAR T cells before co-culture with GD2-CAR T cells and SB28 tumor cells. (**b**) Percentage of dead SB28 tumor cells after co-culture with GD2-CAR T cells at effector:target ratios of 1:1 and 3:1, in the presence of BMDM pretreated with UTD or TREM2 CAR T cells (n=6 replicates from two independent experiments, two-way ANOVA with Bonferroni correction). (**b**) Quantification of IFN-γ secretion (pg/mL) by GD2-CAR T cells measured from the same co-culture experiments shown in (**a**) (n=6 replicates from two independent experiments, two-way ANOVA with Bonferroni correction). (**c**) Left: representative histograms of CFSE dilution in GD2 CAR T cells after co-culture, showing proliferative capacity. Right: Quantification of $CFSE^+$ GD2 CAR T cells expressed as percentage of $CD3^+$ T cells (n=6 replicates from two independent experiments, one-way ANOVA with Bonferroni correction). (**d**) Frequency of effector T cells (T_{eff}, $CD44^+CD62L^-$), central memory T cells (T_{cm}; $CD44^+CD62L^+$), and naïve T cells ($CD44^-CD62L^+$) among GD2 CAR T cells in co-culture with UTD or TREM2 CAR T cell–pretreated BMDM (n=3 replicates, one-way ANOVA with Bonferroni correction). Data are shown as mean ± SEM. *p < 0.05, **p<001, ***p < 0.001.

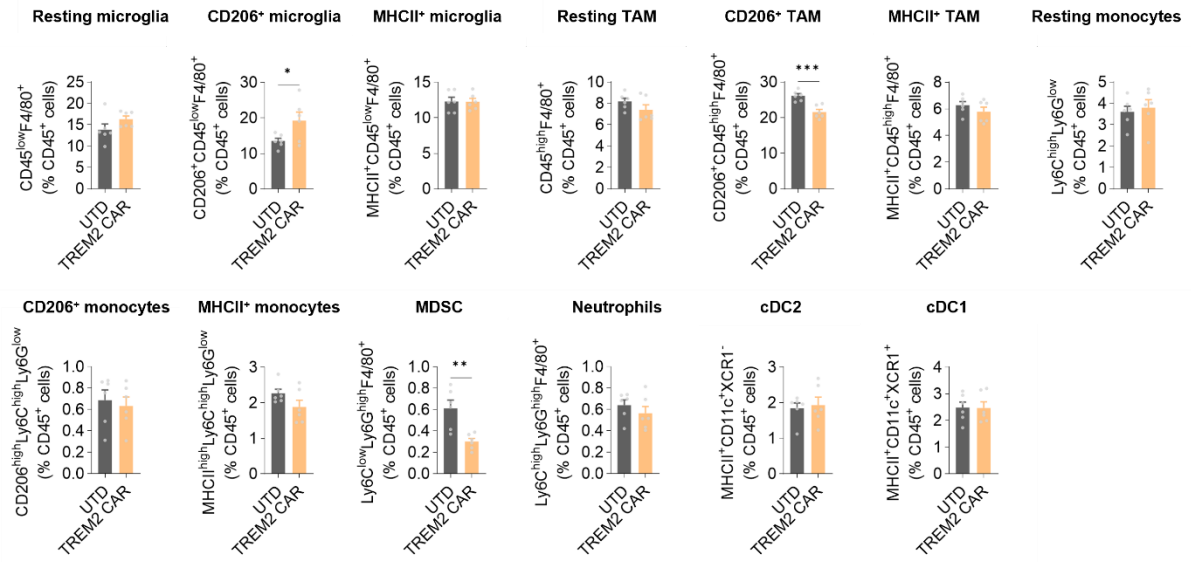

Supplemental figure 13. Myeloid cell remodeling following combined TREM2 and GD2 CAR T-cell therapy in SB28 glioblastoma. Frequency of microglial, dendritic cell (cDC1 and cDC2), myeloid-derived suppressor cells (MDSC), neutrophil, tumor-associated macrophage (TAM), and monocyte subsets in SB28 tumors treated with GD2 CAR T cells combined with untransduced (UTD) or TREM2 CAR T cells shown as percentage of $CD45^+$ cells (n=6 mice per group). Data are shown as mean ± SEM. Unpaired two-tailed t-tests were used. *$p < 0.05$, **$p < 0.01$.

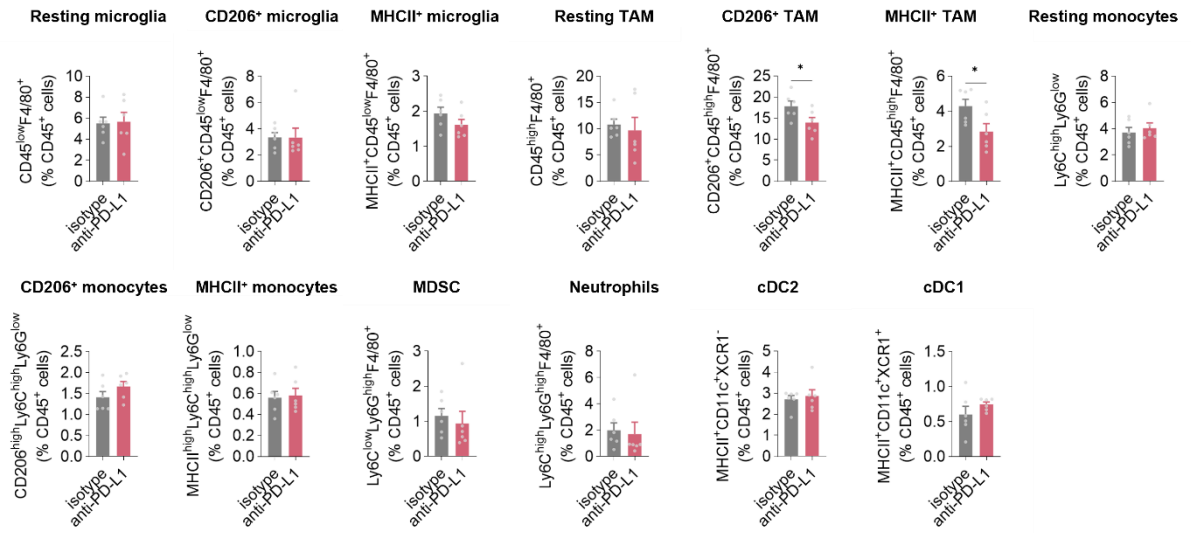

Supplemental figure 14. Effect of locoregional injection of GD2- and TREM2-targeting CAR T cells combined with anti-PD-L1 in SB28 model on TME. Frequency of microglial, dendritic cell (cDC1 and cDC2), myeloid-derived suppressor cells (MDSC), neutrophil, tumor-associated macrophage (TAM), and monocyte subsets in SB28 tumors treated with TREM2/GD2 CAR T cell combined with antiPD-L1 antibody or isotype control shown as percentage of $CD45^+$ cells (n=6 mice per group). Data are shown as mean ± SEM. Unpaired two-tailed t-tests were used. *$p < 0.05$.

Supplemental figure 15. Neoadjuvant GD2 CAR T cell therapy enhances tumor control and prolongs survival in CT2A model. (**a**) Kaplan–Meier survival analysis of CT2A-bearing mice receiving resection alone, adjuvant GD2 CAR T cells, or neoadjuvant GD2 CAR T cells (log-rank test). mOS=median of survival. (**b**) Longitudinal bioluminescence imaging (BLI) quantification of tumor growth in the three treatment groups (n = 12-17 mice per group).

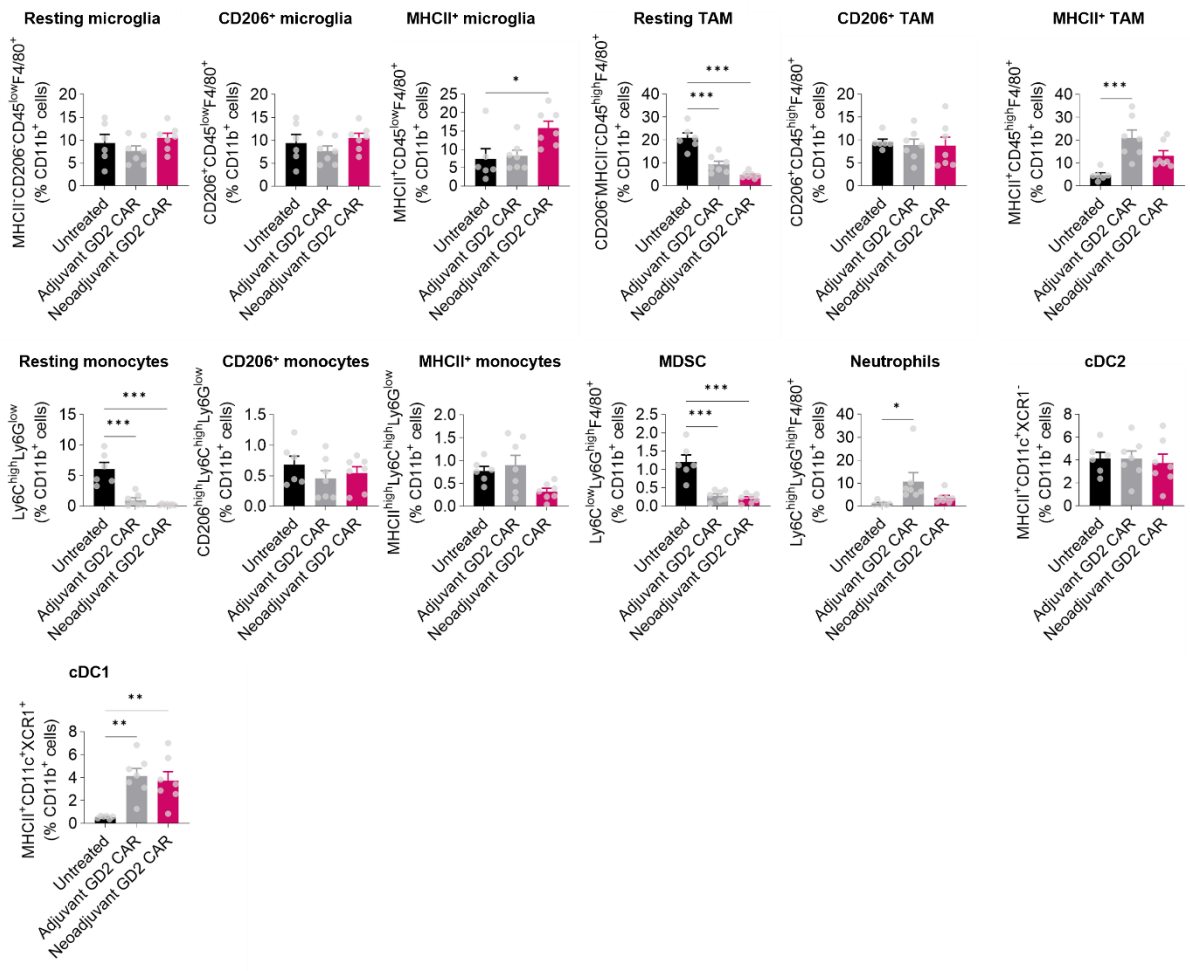

Supplemental figure 16. Myeloid cell compartment remodeling following neoadjuvant versus adjuvant GD2 CAR T-cell therapy in the SB28 model. Frequency of microglial, dendritic cell (cDC1 and cDC2), myeloid-derived suppressor cells (MDSC), neutrophil, tumor-associated macrophage (TAM), and monocyte of resected SB28-bearing mice treated or not with adjuvant or neoadjuvant GD2 CAR T cells. Data are shown as mean ± SEM (n=6-7 per condition, unpaired t-test). *p<0.05, **p<0.01, ***p<0.001.

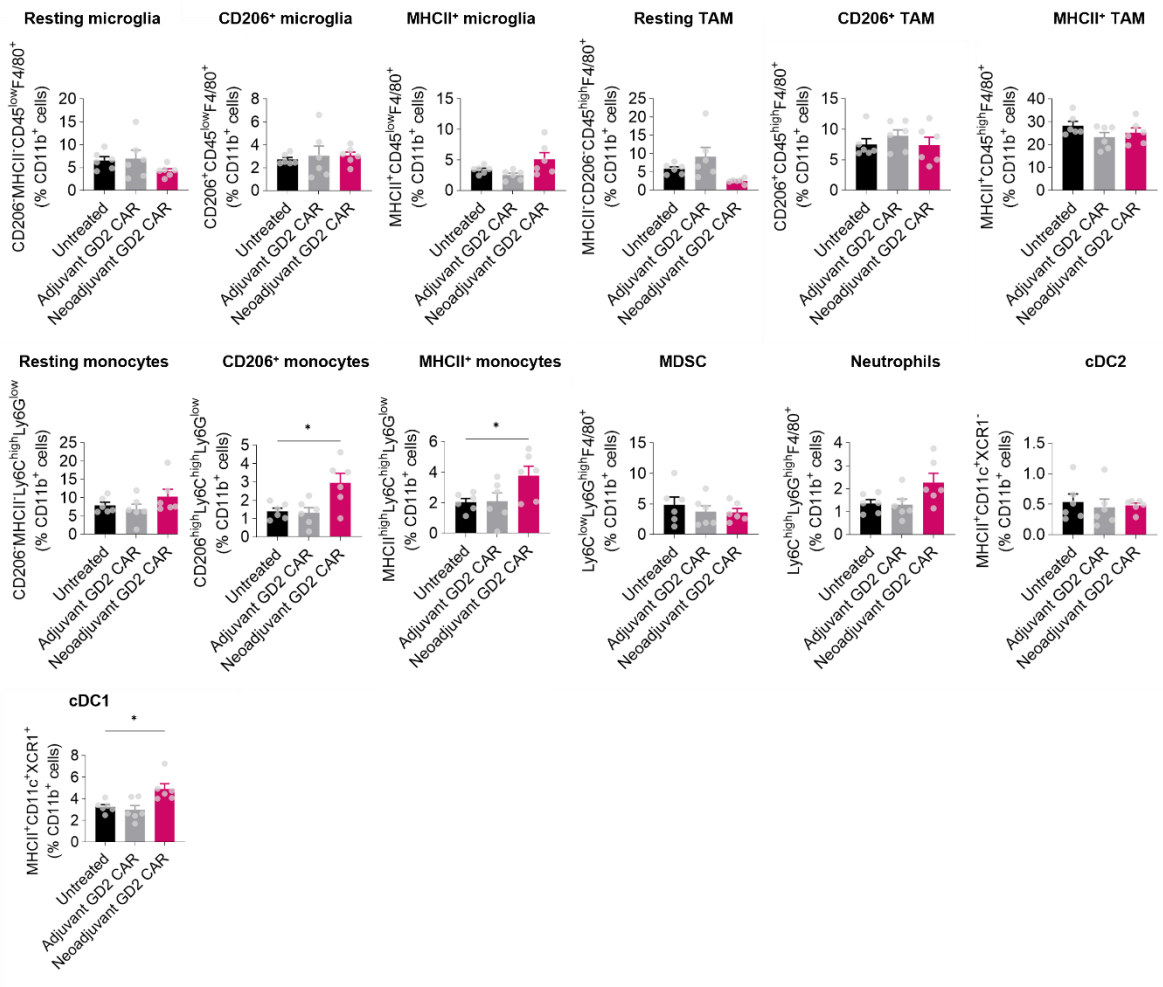

Supplemental figure 17. Myeloid cell compartment remodeling following neoadjuvant versus adjuvant GD2 CAR T-cell therapy in the CT2A model. Frequency of microglial, dendritic cell (cDC1 and cDC2), myeloid-derived suppressor cells (MDSC), neutrophil, tumor-associated macrophage (TAM), and monocyte of resected CT2A-bearing mice treated or not with adjuvant or neoadjuvant GD2 CAR T cells. Data are shown as mean ± SEM (n=6 per condition, unpaired t-test). *p<0.05, **p<0.01, ***p<0.001.

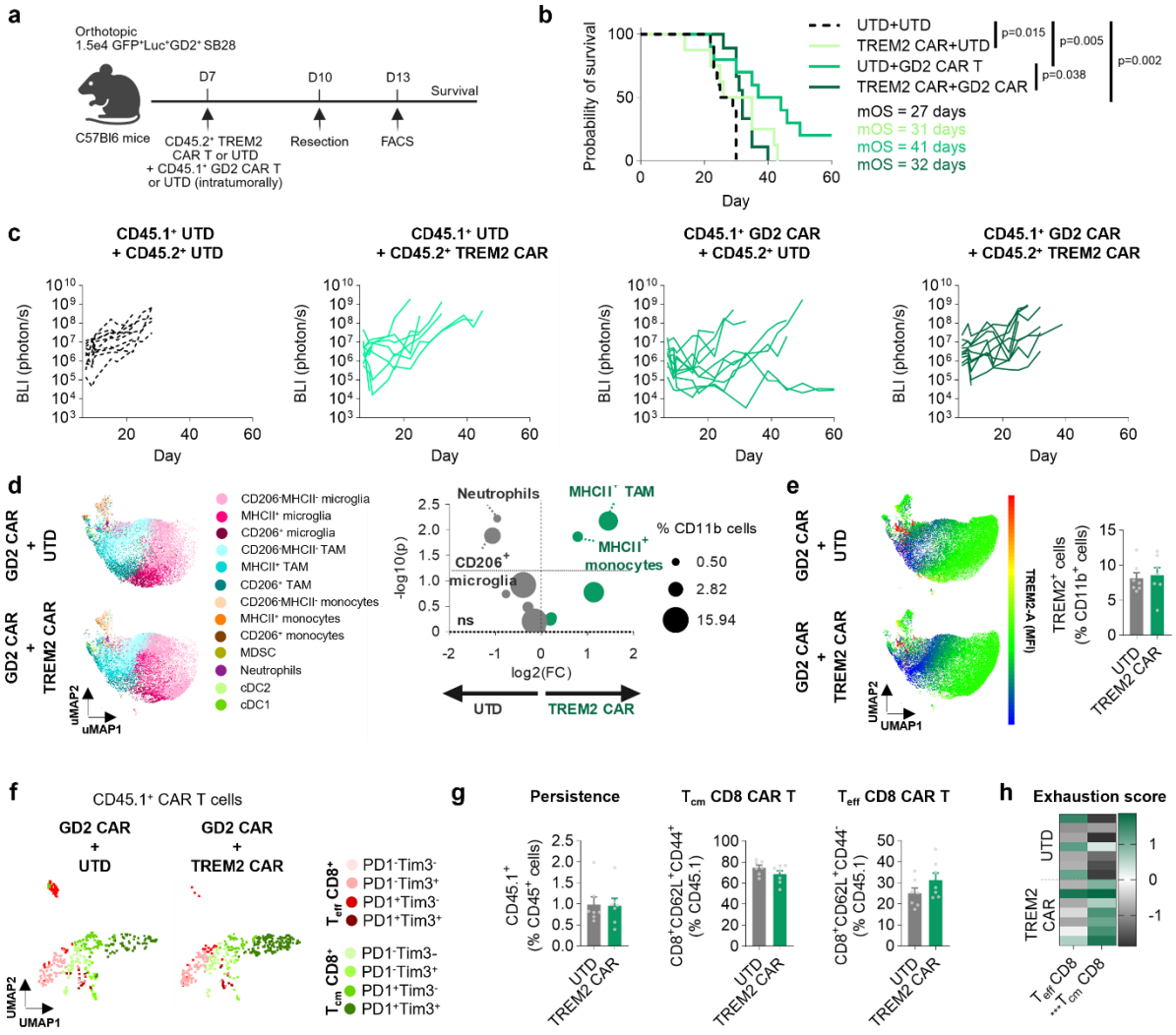

Supplemental figure 18. Effect of combining TREM2 and GD2 CAR T cells as neoadjuvant therapy in SB28 GBM. (**a**) Experimental scheme of SB28-bearing mice treated with two T-cell populations (5×10^5 each): untransduced (UTD)+UTD, antiTREM2 CAR+UTD, UTD+antiGD2 CAR, or antiTREM2 CAR+antiGD2 delivered intratumorally as neoadjuvant on day 7 and resected on day 10. (**b**) Kaplan–Meier survival analysis of mice receiving the indicated neoadjuvant regimens (n=8-10 per group; log-rank test). mOS=median of survival. (**c**) Longitudinal bioluminescence imaging (BLI) quantification of tumor growth in individual mice from each treatment group. (**d**) Uniform manifold approximation and projection (UMAP) visualization of tumor infiltrating $CD11b^+CD45^+$ myeloid cells three days after resection in the UTD+GD2 CAR and TREM2 CAR+GD2 neoadjuvant treatments (left). Volcano plot (right) showing log2 fold-changes (log2(FC)) and mean frequencies of major myeloid cell subsets in TREM2 CAR or UTD T cell-treated mice receiving GD2 CAR T cells. (**e**) Left: UMAP visualization and quantification of TREM2 expression among $CD11b^+CD45^+$ myeloid cells three days post-resection in TREM2 CAR or UTD T cell-treated mice receiving GD2 CAR T cells. Right: flow cytometry quantification of $TREM2^+$ cells among $CD11b^+$ cells in TREM2 CAR or UTD T cell-treated mice receiving GD2 CAR T cells (n=7, unpaired two-tailed t-test). (**f**) UMAP of tumor-infiltrating $CD8^+CD45.1^+$ GD2 CAR T cells colored by manually annotated clusters following TREM2 CAR or UTD T cell treatment. (**g**) Flow cytometry quantification of $CD45.1^+$ CAR T cells among $CD4^+/CD8^+CD45^+$ cells and quantification of T_{eff} CD8

($CD8^+CD62L^-CD44^+$) and T_{cm} CD8 ($CD8^+CD62L^+CD44^+$) among $CD45.1^+$ GD2 CAR T cells in tumors of antiGD2 CAR T cells treated in combination with UTD or antiTREM2 CAR T cells (n=7, unpaired two-tailed t-test). (**h**) Heatmap of exhaustion score (z-score; composite of exhaustion-associated markers, see Methods) for T_{eff} and T_{cm} $CD8^+CD45.1^+$ GD2 CAR T cells (n=7 mice/condition, unpaired t-test). Data are shown as mean ± SEM. ***p<0.001.

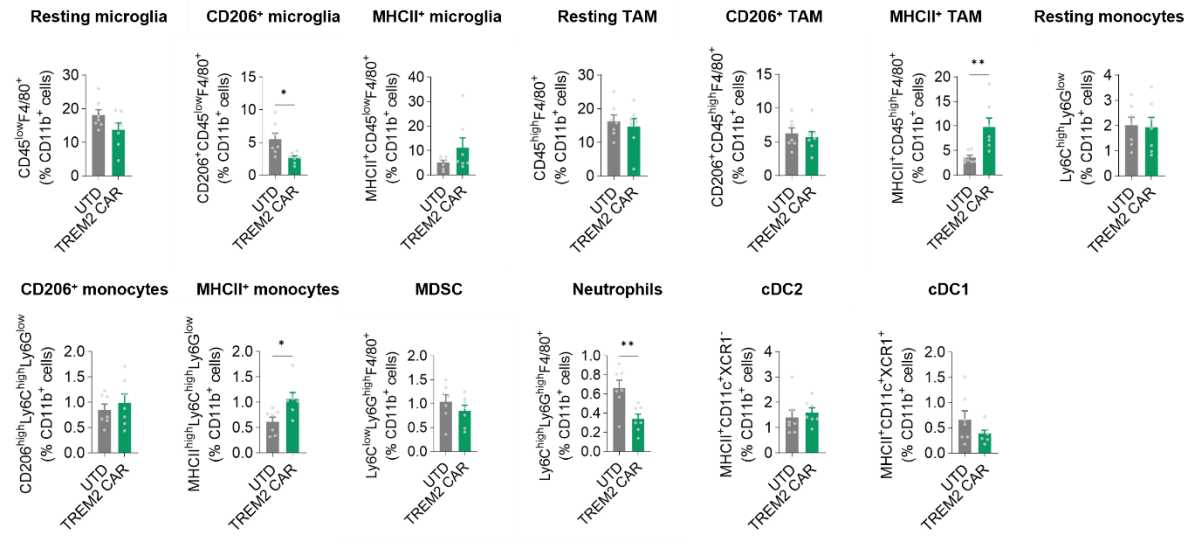

Supplemental figure 19. Effect of co-injection of TREM2 and GD2 CAR T cells as neoadjuvant on the TME in the SB28 model. Frequency of microglial, dendritic cell (cDC1 and cDC2), myeloid-derived suppressor cells (MDSC), neutrophil, tumor-associated macrophage (TAM), and monocyte of GD2 CAR T cell-treated mice bearing SB28 tumor receiving untransduced (UTD) or TREM2 CAR T cells as neoadjuvant (day 7, three days before resection). Data are shown as mean ± SEM (n=7/condition, unpaired t-test). *p<0.05, **p<0.01.

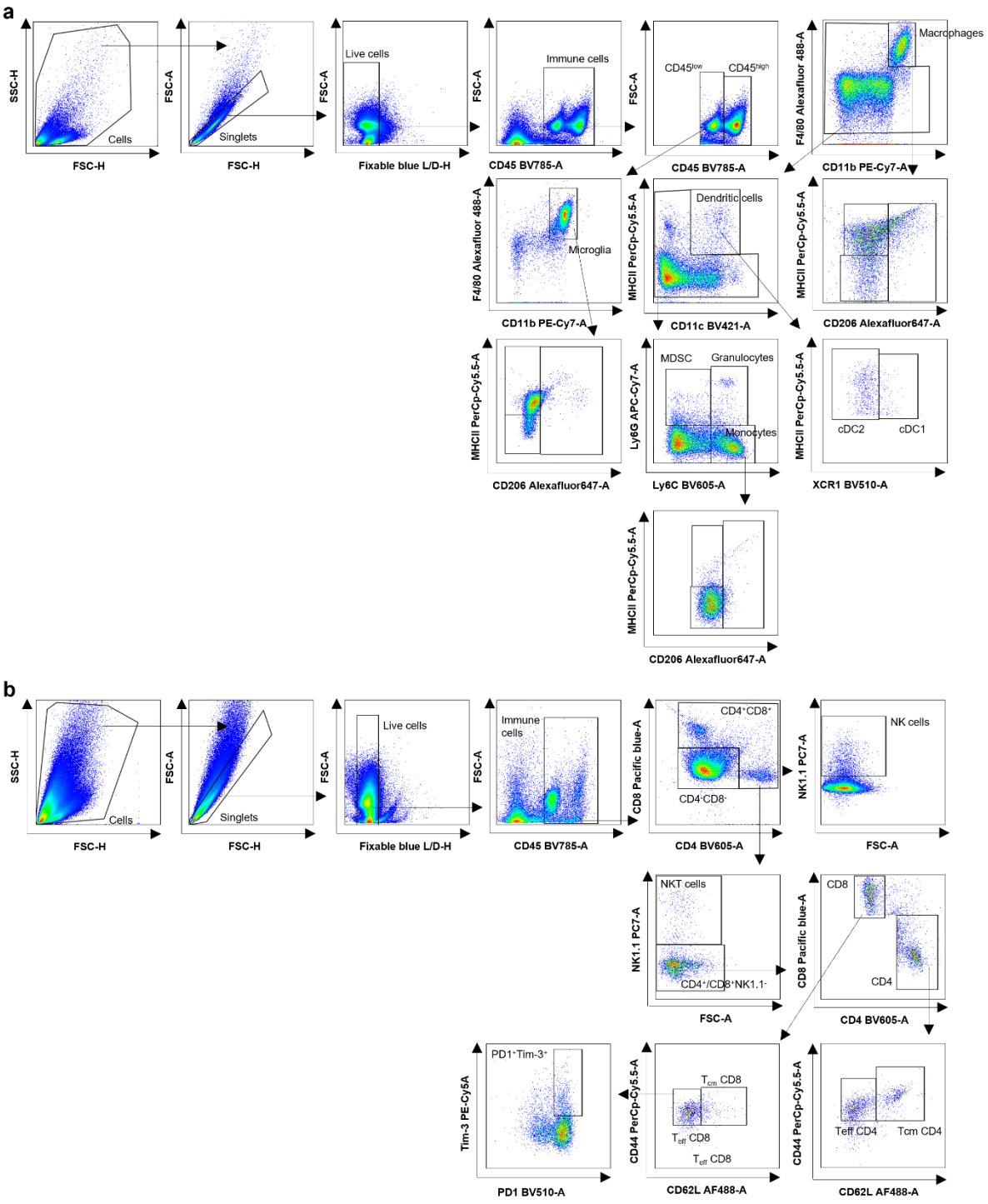

Supplemental Figure 20. Gating strategy for flow cytometry analysis of myeloid and lymphoid cell populations. (**a**) Representative gating strategy for myeloid cell subsets. (**b**) Representative gating strategy for lymphoid cell subsets.

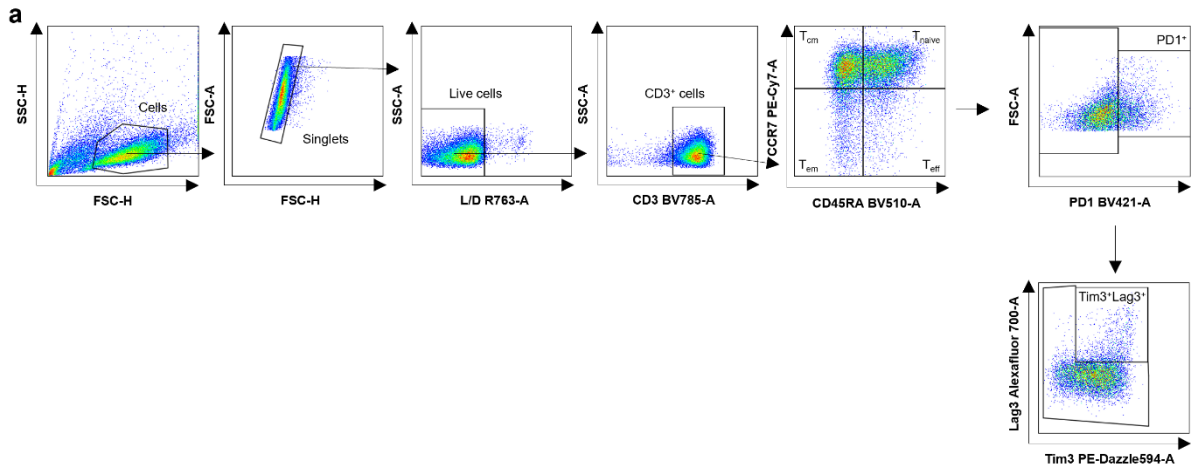

Supplementary figure 21. Gating strategy for flow analysis of human lymphoid subsets. Representative gating strategy for human lymphoid cell subsets.

Antigen	Fluorochrome	Reactivity	Clone	Provider	Reference	Dilution used	Validation
CD16/32	Unconjugated	Mouse	93	Biolegend	101301	1 :100	https://www.biolegend.com/en-us/products/purified-anti-mouse-cd16-32-antibody-190#productCertificate
CD45	BV785	Mouse	30-F11	Biolegend	103149	1 :100	https://www.biolegend.com/en-us/products/brilliant-violet-785-anti-mouse-cd45-antibody-10636
CD11b	PE-Cy7	Mouse/Human	M1/70	Biolegend	101216	1 :100	https://www.biolegend.com/en-us/products/pe-cyanine7-anti-mouse-human-cd11b-antibody-1921
F4/80	Alexafluor 488	Mouse	BM8	Biolegend	123120	1 :100	https://www.biolegend.com/en-us/products/alexa-fluor-488-anti-mouse-f4-80-antibody-4073
I-A/I-E	PerCp/Cy5.5	Mouse	M5/114.15.2	Biolegend	107626	1 :100	https://www.biolegend.com/en-us/products/percp-cyanine5-5-anti-mouse-i-a-i-e-antibody-4282
CD11c	BV421	Mouse	N418	Biolegend	117330	1 :100	https://www.biolegend.com/en-us/products/brilliant-violet-421-anti-mouse-cd11c-antibody-7149
CD206	Alexafluor 647	Mouse	C068C2	Biolegend	141712	1 :50	https://www.biolegend.com/en-us/products/alexa-fluor-647-anti-mouse-cd206-mmr-antibody-7427
Ly6C	BV605	Mouse	HK1.4	Biolegend	128036	1 :100	https://www.biolegend.com/en-us/products/brilliant-violet-605-anti-mouse-ly-6c-antibody-8727
Ly6G	APC-Cy7	Mouse	1A8	Biolegend	127624	1 :100	https://www.biolegend.com/en-us/products/apc-cyanine7-anti-mouse-ly-6g-antibody-6755
XCR1	BV510	Mouse	ZET	Biolegend	148218	1 :100	https://www.biolegend.com/en-us/products/brilliant-violet-510-anti-mouse-rat-xcr1-antibody-10751
TREM2	PE	Mouse	6E9	Biolegend	824805	1 :100	https://www.biolegend.com/en-us/products/pe-anti-trem-2-antibody-22902
CD3	APC-Cy7	Mouse	17A2	Biolegend	100222	1 :100	https://www.biolegend.com/en-us/products/apc-cyanine7-anti-mouse-cd3-antibody-6068
CD8	Pacific Blue	Mouse	53-6.7	Biolegend	100725	1 :100	https://www.biolegend.com/en-us/products/pacific-blue-anti-mouse-cd8a-antibody-2856
CD4	BV605	Mouse	GK1.5	Biolegend	100451	1 :100	https://www.biolegend.com/en-us/products/brilliant-violet-605-anti-mouse-cd4-antibody-10708
NK1.1	PC7	Mouse	PK136	Biolegend	108714	1 :100	https://www.biolegend.com/en-us/products/pe-cyanine7-anti-mouse-nk-1-1-antibody-2840
CD44	PerCp	Mouse/Human	IM7	Biolegend	103036	1 :100	https://www.biolegend.com/en-us/products/percp-anti-mouse-human-cd44-antibody-6895
CD62L	Alexafluor 488	Mouse	MEL-14	Biolegend	104420	1 :100	https://www.biolegend.com/en-us/products/alexa-fluor-488-anti-mouse-cd62l-antibody-3115
PD-1	BV510	Mouse	29F.1A12	Biolegend	135241	1 :100	https://www.biolegend.com/en-us/products/brilliant-violet-510-anti-mouse-cd279-pd-1-antibody-14923
Tim-3	PE	Mouse	B8.2C12	Biolegend	134004	1 :100	https://www.biolegend.com/en-us/products/pe-anti-mouse-cd366-tim-3-antibody-5908
CD45.1	PerCp-Cy5.5	Mouse	A20	BD Biosciences	560580	1 :100	https://www.bdbiosciences.com/en-eu/products/reagents/flow-cytometry-reagents/research-reagents/single-color-antibodies-ruo/percp-cy-5-5-mouse-anti-mouse-cd45-1.560580
CD45.2	BV785	Mouse	104	Biolegend	109839	1 :100	https://www.biolegend.com/en-us/products/brilliant-violet-785-anti-mouse-cd45-2-antibody-8924
PD-L1	BV785	Mouse	10F.9G2	Biolegend	124331	1 :100	https://www.biolegend.com/en-us/products/brilliant-violet-785-anti-mouse-cd274-b7-h1-pd-l1-antibody-13497
iNOS	PE	Mouse	CXNFT	Thermofisher	12-5920-82	1 :100	https://www.thermofisher.com/antibody/product/iNOS-Antibody-clone-CXNFT-Monoclonal/12-5920-82
Arginase-1	APC	Mouse	A1exF5	Thermofisher	17-3697-82	1 :100	https://www.thermofisher.com/antibody/product/Arginase-1-Antibody-clone-A1exF5-Monoclonal/17-3697-82
TREM2	Alexafluor 647	Mouse/Human	237920	R&D Systems	FAB17291R-025	1 :50	https://www.rndsystems.com/products/human-mouse-trem2-alexa-fluor-647-conjugated-antibody-237920_fab17291r
F4/80	BV421	Mouse	BM8	Biolegend	123137	1 :100	https://www.biolegend.com/en-us/products/brilliant-violet-421-anti-mouse-f4-80-antibody-7199
CD206	BV605	Mouse	C068C2	Biolegend	141721	1 :50	https://www.biolegend.com/en-us/products/brilliant-violet-605-anti-mouse-cd206-mmr-antibody-8729
CD11c	BV711	Mouse	N418	Biolegend	117349	1 :100	https://www.biolegend.com/en-us/products/brilliant-violet-711-anti-mouse-cd11c-antibody-10175
PD-L1	BV785	Mouse	10F.9G2	Biolegend	124331	1 :100	https://www.biolegend.com/en-us/products/brilliant-violet-785-anti-mouse-cd274-b7-h1-pd-l1-antibody-13497
CXCR2	APC	Mouse	M5/114.15.2	Biolegend	149312	1 :100	https://www.biolegend.com/en-us/products/apc-anti-mouse-cd182-antibody-15676
CD66a	APC-Cy7	Mouse	10F.9G2	Biolegend	134540	1 :100	https://www.biolegend.com/en-us/products/apccyanine7-anti-mouse-cd66a-ceacam1a-antibody-19636
CD44	BV510	Mouse	M1/70	Biolegend	103044	1 :100	https://www.biolegend.com/en-us/products/brilliant-violet-510-anti-mouse-human-cd44-antibody-7994
Ly6G	BV421	Mouse	1A8	Thermofisher	404-9668-82	1 :100	https://www.thermofisher.com/antibody/product/Ly-6G-Antibody-clone-1A8-Ly6g-Monoclonal/404-9668-82
Ly6C	PerCp/Cy5.5	Mouse	MAb-CC1	Biolegend	128012	1 :100	https://www.biolegend.com/en-us/products/percp-cyanine5-5-anti-mouse-ly-6c-antibody-5967
Arginase-1	FITC	Mouse	A1exF5	Thermofisher	53-3697-82	1 :100	https://www.thermofisher.com/antibody/product/Arginase-1-Antibody-clone-A1exF5-Monoclonal/53-3697-82
CD62L	PE-Cy7	Mouse	HK1.4	Biolegend	104418	1 :100	https://www.biolegend.com/en-us/products/pe-cyanine7-anti-mouse-cd62l-antibody-1922
I-A/I-E	BV785	Mouse	SA044G4	Biolegend	107645	1 :100	https://www.biolegend.com/en-us/products/brilliant-violet-785-anti-mouse-i-a-i-e-antibody-12087
PD-L1	PE	Mouse	10F.9G2	Biolegend	124308	1 :100	https://www.biolegend.com/en-us/products/pe-anti-mouse-cd274-b7-h1-pd-l1-antibody-4497
F4/80	PE	Mouse	W20065B	Biolegend	111604	1 :100	https://www.biolegend.com/en-us/products/pe-anti-mouse-f4-80-antibody-23902
PD-L1	BV510	Mouse	10F.9G2	BD Biosciences	571067	1 :100	https://www.bdbiosciences.com/en-de/products/reagents/flow-cytometry-reagents/research-reagents/single-color-antibodies-ruo/BV510-Rat-Anti-Mouse-CD274-(PD-L1).571067?tab=product_details
CD3	BV785	Human	SK7	Biolegend	344842	1 :100	https://www.biolegend.com/en-us/products/brilliant-violet-785-anti-human-cd3-antibody-13305
CD197 (CCR7)	PE-Cy7	Human	G043H7	Biolegend	353226	1 :100	https://www.biolegend.com/en-us/products/pecyanine7-anti-human-cd197-ccr7-antibody-7694
CD45RA	BV510	Human	HI100	Biolegend	304142	1 :100	https://www.biolegend.com/en-us/products/brilliant-violet-510-anti-human-cd45ra-antibody-8007
PD-1	BV421	Human	EH12.2H7	Biolegend	329920	1 :100	https://www.biolegend.com/en-us/products/brilliant-violet-421-anti-human-cd279-pd-1-antibody-7191

Tim-3	PE-CF594	Human	7D3	BD Biosciences	2059595	1 :100	https://www.bdbiosciences.com/en-pl/products/reagents/flow-cytometry-reagents/research-reagents/single-color-antibodies-ruo/pe-cf594-mouse-anti-human-tim-3-cd366.565560?tab=product_details
Lag-3	Alexafluor 700	Human	11C3C65	Biolegend	369344	1 :100	https://www.biolegend.com/en-us/products/alexa-fluor-reg-700-anti-human-cd223-lag-3-21598
CD68	Alexafluor 555	Human	KP1	Thermofisher	754068882	1 :200	https://www.thermofisher.com/antibody/product/CD68-Antibody-clone-KP1-Monoclonal/754-0688-82
HLA-DR	Alexafluor 488	Human	LN3	Biolegend	327010	1 :200	https://www.biolegend.com/en-us/products/alexa-fluor-488-anti-human-hla-dr-antibody-4167

Table 1.

Gene	Forward primer (5'→3')	Reverse primer (5'→3')
Eef1a1	ACGAGGCAATGTTGCTGGTGAC	GTGTGACAATCCAGAACAGGAGC
Arginase 1	TTTTAGGGTTACGGCCGGTG	CCTCGAGGCTGTCCTTTTGA
Il10	GGTTGCCAAGCCTTATCGGA	GGGGAGAAATCGATGACAGC
Cd206	GTTCACCTGGAGTGATGGTTCTC	AGGACATGCCAGGGTCACCTTT
Cd163	GGCTAGACGAAGTCATCTGCAC	CTTCGTTGGTCAGCCTCAGAGA
Tgfb	TGACGTCACTGGAGTTGTACGG	GGTTCATGTCATGGATGGTGC
Cd86	TGTTTCCGTGGAGACGCA	TTGAGCCTTTGTAAATGG
Inos	GCCACCAACAATGGCAACAT	TCGATGCACAACTGGGTGAA
Cxcl10	ATCATCCCTGCGAGCCTATCCT	GACCTTTTTTGGCTAAACGCTTTC
Trem2	CTACCAGTGTCAGAGTCTCCGA	CCTCGAAACTCGATGACTCCTC

Table 2.